Frame format and DSP receiver design for a 56-GBaud GEO DP-QPSK coherent optical feeder link

Raphaël Le Bidan, Hugo Meric, Julien Sommer

Frame format and DSP receiver design for a 56-GBaud GEO DP-QPSK coherent optical feeder link

Raphaël Le Bidan
Lab-STICC UMR 6285
IMT Atlantique, MEE Dept.
Brest, France
raphael.lebidan@imt-atlantique.fr

Hugo Meric
CNES
Toulouse, France
hugo.meric@cnes.fr

Julien Sommer
CNES
Toulouse, France
julien.sommer@cnes.fr

***Abstract*—This paper addresses the design of a custom digital signal processing receiver and companion frame format for a 56 GBaud coherent optical Dual-Polarization Quadrature Phase-Shift Keying GEO feeder link. The selected algorithms combine standard practice from both coherent optical fiber and RF satellite communications. Robust blind algorithms are used in the first stages, followed by data-aided algorithms for subsequent fine carrier and phase recovery. A simplified blind equalizer architecture is proposed for fast and robust polarization demultiplexing, based on a modified constant-modulus algorithm. Our simulations demonstrate the possibility to establish links at an electrical SNR as low as -6 dB, in the presence of realistic values of system impairments, using less than 5% signaling overhead.**

***Index Terms*—GEO feeder link, coherent detection, digital signal processing, synchronization, equalization**

I. Introduction

Satellite communications systems require to reduce the overall cost per bit in order to remain competitive with terrestrial solutions and to offer affordable high-speed Internet services. Replacing or complementing radio-frequency (RF) feeder links by optical links is regarded as a promising solution to cope with the increasing RF bandwidth scarcity problem. Free-space optical (FSO) communications are expected to deliver substantially higher data rates than RF-based solutions, by an order of magnitude at least, with less interference, and comparable onboard terminal footprint [1], [2].

In 2018, the French space agency CNES initiated a study to analyze the technical and economic feasibility of optical feeder links for geostationary (GEO) satellites. After evaluating several trade-offs (telescope size, waveform, etc.) from a system point of view, a series of technical recommendations were issued, accompanied by a roadmap to develop the corresponding technological building blocks: optical amplifiers, multiplexers, modems, etc. A coherent 56-GBaud dual-polarization QPSK (DP-QPSK) waveform was selected at the physical layer, as a good compromise between achievable throughput, increased receiver sensitivity, expected robustness against atmospheric turbulence, and long-term evolution capabilities. We note that discussions are currently underway at the CCSDS Optical Communications Working Group to incorporate coherent signaling in a revision of the Blue Books.

In principle, the use of 1550 nm lasers makes it possible to leveraging some of the commercial off-the-shelf (COTS) optical components and 100G/400G coherent transceiver subsystems developed for terrestrial fiber-optic networks. The problem is that they are designed to cope with different impairments than those encountered in space optical links. COTS coherent transceivers are mainly interference-limited. They are intended to operate at high signal-to-noise ratio (SNR), and a large part of the baseband digital-signal-processing (DSP) receiver is dedicated to the compensation of the interference introduced by linear (chromatic dispersion and polarization-mode dispersion) and non-linear fiber impairments. On the other hand, space optical communications are primarily power-limited. The development of high-power optical amplifiers for long-distance GEO links through the atmosphere proves to be challenging, and the modem has to be able to lock at very low electrical SNR (< 0 dB). This raises the question of the extent to which it is possible to re-use the signal formats and DSP algorithms developed for coherent fiber-optic communications in such conditions. Recently, the authors of [3] have successfully demonstrated 100-Gbps and 200-Gbps laser LEO communication downlinks, based on COTS DP-QPSK transceivers supplemented by an automatic repeat request (ARQ) protocol to mitigate the effects of atmospheric turbulence. While very cost effective in the LEO setting, this approach does not come without limitations for high-capacity coherent optical GEO feeder links, which may have much to benefit from a custom receiver architecture [4], [5].

This paper reports on a second study supported by the CNES, that addressed the problem of designing a dedicated frame format and DSP receiver for the selected 56-GBaud DP-QPSK GEO feeder scenario. It is organized as follows. Section II provides an overview of the communication link model, performance requirements, and design goals of the project. Section III details the proposed frame format and receiver architecture. The selected DSP algorithms are reviewed in Section IV. Simulation results are presented in Section V.

II. Link model and design requirements

A. Transmission scenario

The communication link under consideration is depicted in Fig. 1. Transmission uses DP-QPSK signaling at symbol rate $R_s = 56$ GBaud, with a square-root raised cosine pulse-shape having a very small roll-off factor $\alpha = 0.1$. Prior

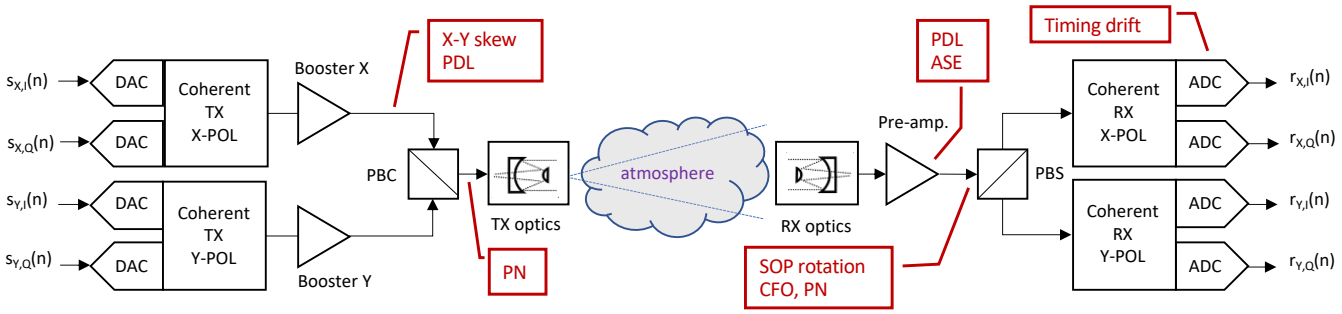

Fig. 1. Transmission model (CFO = carrier-frequency offset, PN = laser phase noise, ASE = optical amplification noise, PDL = polarization dependent loss).

system studies conducted by the CNES concluded that, apart from atmospheric turbulence, the main impairments to be considered or addressed in the digital receiver design were:

- polarization time skew (X-Y skew) induced by separate optical pre-amplification of the two polarizations at the transmitter;
- polarization-dependent losses (PDL) introduced by the optical transmit and receive subsystems;
- accumulated laser phase noise (PN) from the transmit laser and receive local oscillator (LO);
- an unknown and possibly time-varying state-of-polarization (SOP) rotation at the receive LO;
- a carrier-frequency offset (CFO) at the receive LO;
- optical amplified spontaneous emission (ASE) noise;
- timing drift in the analog-to-digital converters (ADCs)

A discrete-time over-sampled channel model of the link has been developed, capturing all the above-mentioned impairments. Following standard practice, we used a Wiener phase noise model for the laser phase noise, and a white gaussian noise model for ASE noise. Atmospheric turbulence was not explicitly simulated in this work, as it fluctuates at a time scale much larger than the frame duration, and the fading caused by scintillation cannot be compensated by DSP algorithms alone, but rather through adaptive optics, forward-error-correction (FEC) coding and interleaving, or other forms of diversity.

B. Performance requirements

The following performance requirements were specified:

- maximum X-Y skew tolerance of 0.25 ns;
- peak PDL tolerance of 5 dB;
- maximum cumulated -3dB bandwidth $\Delta\nu = 600$ kHz for the laser phase noise;
- maximum CFO of ± 5 GHz;
- tolerance of timing clock drift up to ± 30 ppm;
- minimum operating electrical SNR $E_s/N_0 = -6$ dB

The large X-Y polarization time skew arising from the use of distinct transmit amplifiers for each polarization, which may span up to 15 symbol periods, is a notable difference with fiber-optic communications. Another one is the minimum electrical SNR of -6 dB, which translates into a received optical power in the range $-60 \leq \text{ROP} \leq -55$ dBm for typical optical receiver front-ends. Our discrete-time equivalent channel model does not simulate atmospheric turbulence. Yet scintillation is tacitly taken into account in this minimum operating SNR level, which includes sufficient margin to ensure reliable communication at the desired average throughput, with the envisioned FEC code and interleaver, in conditions of turbulence that are typical of GEO links.

C. Design goals and constraints

The present work had two main objectives: i) to propose a frame format and a comprehensive DSP receiver for the transmission scenario of Fig. 1, and ii) to evaluate its performance against the specified performance requirements. The proposed DSP algorithms should have low latency and be amenable to parallel processing in order to comply with the 56 GBaud symbol rate constraint. Other practical design constraints included a total overhead for the training sequences and pilot symbols limited to 5% of the symbol rate at most, and DSP receiver processing at no more than 2 samples per symbol, to comply with existing 128-Gs/s commercial ADCs.

The driving motivation behind this work was to assess to what extent can one re-use in outer space the coherent DSP algorithms and chips developed either for high-performance, long-haul optical fiber communications [6] or for low-power, short-reach data center optical interconnects [7].

III. DSP Frame Format and Receiver Architecture

A. Design methodology

We first compared the frame format and baseline receiver architecture for a popular RF satellite communication standard, DVB-S2/S2X [8], and for the only public coherent fiber-optic standard we are aware of, namely the OIF 400ZR agreement for interoperable data center interconnect [9]. 400ZR is designed for low-power short-reach coherent communication at a symbol rate of nearly 60 GBaud, in the presence of a limited amount of fiber dispersion, 120 km at worse, which comes close to our scenario in several aspects. The goal of the comparison was to highlight the convergence points as well as the major differences. RF satellite receivers are not designed to cope with the polarization and other impairments, e.g., laser phase noise, specific to coherent optical transmissions (although cross-polarization equalization can be required also on certain RF channels). On the other hand, the 400ZR DSP

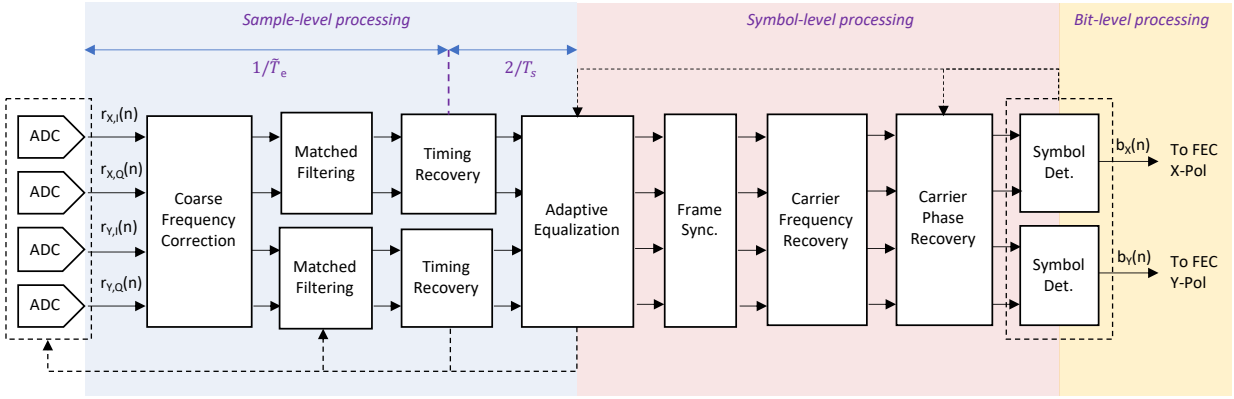

Fig. 2. Block diagram of the DSP receiver (dashed lines show possible feedback paths, not implemented here for latency constraints)

frame and receiver algorithms does not allow for reliable frame acquisition and carrier/phase recovery at the very low SNRs that can be encountered in space optical links. This led us to define a custom frame format and an entire DSP receiver architecture, FEC excluded, that could meet all the constraints and performance requirements of the envisioned GEO link.

B. Frame format

The proposed DSP frame format is depicted in Fig. 3. It achieves a synthesis between DVB-S2 and 400ZR framing. Each frame starts with a known preamble (frame header) of size H symbols, followed by I consecutive packets. Each packet consists of D payload symbols followed by a block of P pilot symbols. Similar to 400ZR, the X and Y polarizations use distinct frame headers and pilot symbol sequences.

As will be demonstrated shortly after, good synchronization and transmission performance can be achieved by choosing $H = 64$, $D = 248$, and $P = 8$. Such a choice has the additional benefit of providing header and packet sizes that are powers of two, which can substantially facilitate parallel processing at the receiver side, *e.g.* through block frequency-domain filtering. The pilots block size $P = 8$ and spacing $D = 248$ result from a trade-off between estimation accuracy and fine tracking capability of the expected worst-case laser phase noise dynamics. We note that 31 symbols only separate (single) pilots in 400ZR. But the latter has been designed for lasers having worse frequency noise characteristics.

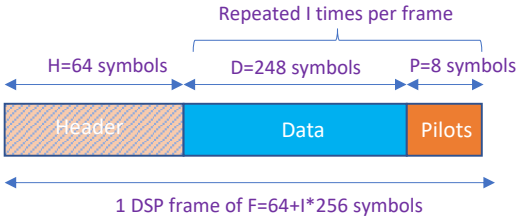

Fig. 3. DSP frame format

Let's take the CCSDS O3K FEC code length as an example. The $n = 30720$ code bits would map onto $I = \lceil 30720/(2 \times 248) \rceil = 62$ packets of 248 QPSK payload symbols. The resulting overhead, neglecting the extra zero-padding in the final packet, would be $\eta = (H + I \times P)/(I \times D) = 3.6\%$, which is fully compliant with our design constraints.

C. DSP receiver architecture

Several candidate DSP solutions have been evaluated and compared at each stage of the digital receiver. The goal was to identify practical and robust DSP algorithms that translate well into high-throughput hardware processing. Accordingly, the choice was made to favor open-loop solutions at each step. The proposed receiver architecture is described in Fig. 2, in which we distinguish between operations performed at the sampling rate (twice the symbol rate in our case), at the symbol rate, and at the bit rate, respectively. Robust blind algorithms are used in the first stages. Data-aided algorithms then follow for the fine carrier and phase recovery steps. Section IV provides details about the purpose of each stage and the selected algorithms.

D. DSP receiver operation

At receiver startup, before regular data demodulation can begin, a fixed period of time is required for blind initialization and training of the coarse frequency correction, timing recovery, and adaptive equalization stages. Our simulations have shown that less than $50\mu s$ was sufficient to achieve steady-state convergence, even at the lowest SNR. Once done, the receiver can enter the frame acquisition process, which could take another $50\mu s$ to complete. All in all, initialization and lock-in was achieved in (usually much) less than $100\mu s$, even in the worst SNR and PDL conditions.

IV. DSP Algorithms

A. Coarse frequency synchronization

At system startup, the initial CFO may be very large. The function of the coarse frequency correction stage is to bring the offset down to a small fraction of the symbol rate. Not

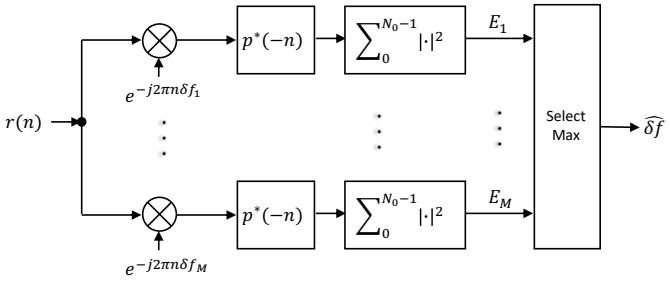

Fig. 4. Principle of coarse frequency-offset estimation

initially foreseen in our receiver design, coarse CFO pre-correction was found to be mandatory in order to avoid a detrimental SNR loss due to mismatched receiver filtering when the CFO exceeded $\pm 0.05 R_s$. The very small roll-factor $\alpha = 0.1$ imposed by project specifications is to blame for this high sensitivity to the CFO. Fortunately, simple and robust open-loop solutions exist, that can handle large CFO without precise knowledge of the symbol timing. We opted for the open-loop non-data-aided (NDA) frequency estimator described in [10, Sec. 3.5.2] and illustrated in Fig. 4. It consists in applying to the received signal a set of M uniformly-spaced tentative CFO corrections $\{\delta f_1, \ldots, \delta f_M\}$, computing the energy of each of the rotated signals over some window of N_0 samples, and choosing as coarse CFO estimate the hypothesis yielding largest energy. Since we have a DP signal and the CFO affects both polarizations in the same way, we collect and sum the total signal energy over the two polarizations. Coarse CFO estimation needs only be done once, during the training period, and is then disabled to save power. The M tentative pre-corrections can be carried out in parallel. Assuming a frequency spacing $\Delta = \delta f_{i+1} - \delta f_i$ between tentative corrections and correct coarse CFO estimation, the residual CFO after coarse estimation and correction will be at most $\pm\Delta/2$. One can trade estimation accuracy and peak CFO tolerance for hardware complexity through the number M of candidate CFO to test. In our simulations, we used $M = 6$ candidate CFOs $\{\pm 0.025, \pm 0.075, \pm 0.125\} \times R_s$, and averaged over $N_0 = 4096$ samples.

B. Matched filtering

Chromatic dispersion is negligible in FSO links. Accordingly, static equalization reduces to simple matched filtering, and can be efficiently carried out by block-filtering in the frequency domain with the overlap-save trick, see *e.g.* [6], [7]. We chose to implement matched filtering prior to timing recovery in order to improve SNR for the latter.

C. Timing recovery

The function of the timing recovery block is to compensate for the sampling clock offset and reconstruct a discrete-time over-sampled signal at exactly twice the symbol rate used at the transmitter. Symbol rate down-sampling will happen later on, at the adaptive equalizer output. Timing recovery is performed block-wise, in the manner shown in Fig. 5, wherein a sampling time offset estimate is calculated for each block, and then corrected by digital interpolation of the block samples. Due to X-Y skew, the sampling time offset will generally be different on the two polarizations, requiring independent timing recovery functions for each. Blind timing estimation under the constraint of feed-forward processing at 2 samples per symbol leaves little choice but Lee's estimator [11], or its asymptotic unbiased variant [12]. When averaging over blocks of 5000 symbols or more, (an equivalent PLL would have a normalized loop bandwidth $B_L T_s \approx 10^{-4}$), this estimator can provide accurate timing correction in the presence of phase noise and CFO, as demonstrated by the mean-square error (MSE) performance in Fig. 6. Other simulations, not reported here, have assessed its robustness to cross-polarization impairments (skew and SOP rotation), as well as its ability to track timing clock drifts of ± 30 ppm.

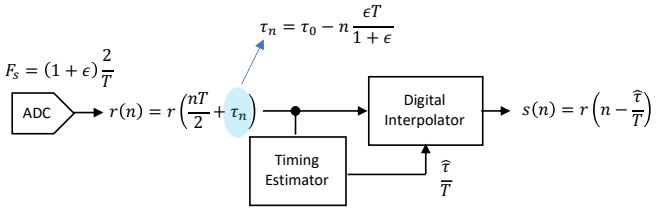

Fig. 5. Block diagram of timing recovery

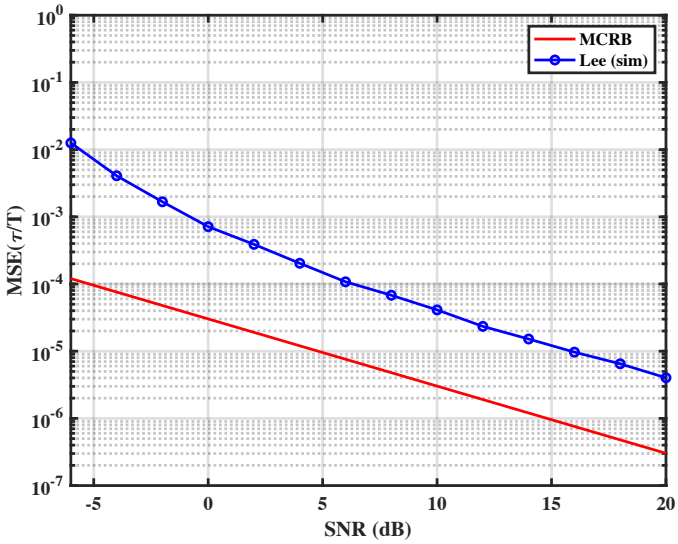

Fig. 6. Mean-square error performance of Lee's timing estimator with a block size of 5000 symbols, a normalized CFO of $0.025/T_s$, and 600 kHz of laser phase noise; Comparison with the modified Cramer-Rao bound (MCRB)

D. Adaptive cross-polarization equalization

As FSO links are not impaired by PMD, we can revisit and simplify the usually power-intensive 2×2 adaptive equalization stage at the core of coherent optical DSP receivers [13]. In

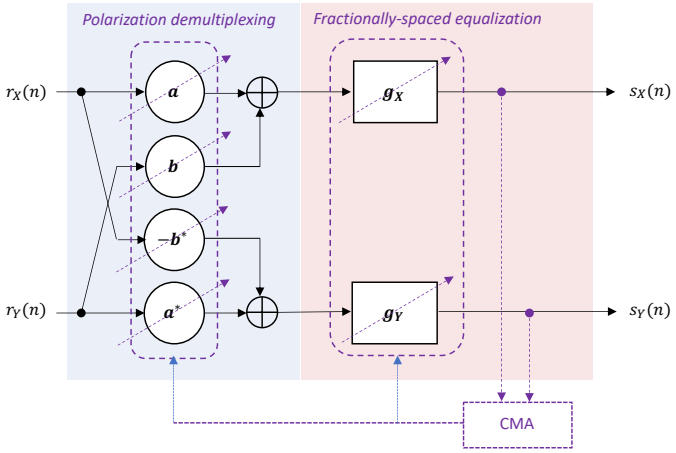

Fig. 7. Structure of the proposed adaptive blind cross-polarization equalizer

the present case, the role of this fractionally-spaced equalizer (FSE) reduces to recovering the SOP, possibly compensating for bandwidth limitations in the opto-electrical front-end, and eventually synthesizing the optimum sampling epoch to return to one sample per symbol period. Accordingly, we propose to use the simplified equalizer structure in Fig. 7. It replace the classical four-filters butterfly arrangement by a 2×2 *scalar* multiplication stage in charge of polarization demultiplexing [14], followed by two adaptive fractionally-spaced filters only, one per polarization. The two complex scalar coefficients (a, b) and two complex-valued filters $(\mathbf{g_X}, \mathbf{g_Y})$ are jointly adapted, based on a regularized constant-modulus algorithm (CMA) criterion that enforces a unitary transform constraint on the first stage. The proposed cost function reads

$$\mathbb{J}(a, b, \mathbf{g_X}, \mathbf{g_Y}) = \mathbb{E}\left(|s_X(n)|^2 - 1\right)^2 + \mathbb{E}\left(|s_Y(n)|^2 - 1\right)^2 + \lambda\left(|a|^2 + |b|^2 - 1\right)^2 \quad (1)$$

where λ is a non-negative real coefficient that balances the relative weight given to the CMA constraint and to the first-stage unit norm constraint, respectively, in the tap coefficients update. Adaptation of the scalar demultiplexing coefficients (a, b) and filter taps for $(\mathbf{g_X}, \mathbf{g_Y})$ uses a standard stochastic gradient descent approximation of the cost function (1). Equalizer adaptation is performed block-wise, to enable fast adaptive frequency-domain filtering [13], [15]. Our simulations used 16-taps filters for $(\mathbf{g_X}, \mathbf{g_Y})$. Equalizer coefficients were adapted once every 32 symbol periods, with step-size parameter $\mu = 10^{-3}$ for training, and $\mu = 5.10^{-4}$ for tracking. Parameter λ was set to 0.7.

Blind equalization was preferred to decision-directed adaptation as the latter can lead to catastrophic error propagation at very low SNR. In addition the use of tentative decisions would require a feedback path from the carrier and phase recovery stages, thereby increasing latency. In contrast, the CMA has the advantage of being insensitive to CFO and phase noise. Owing to its first stage, the proposed equalizer is also structurally immune to the well-known CMA singularity problem, whereby the CMA may happen to converge to

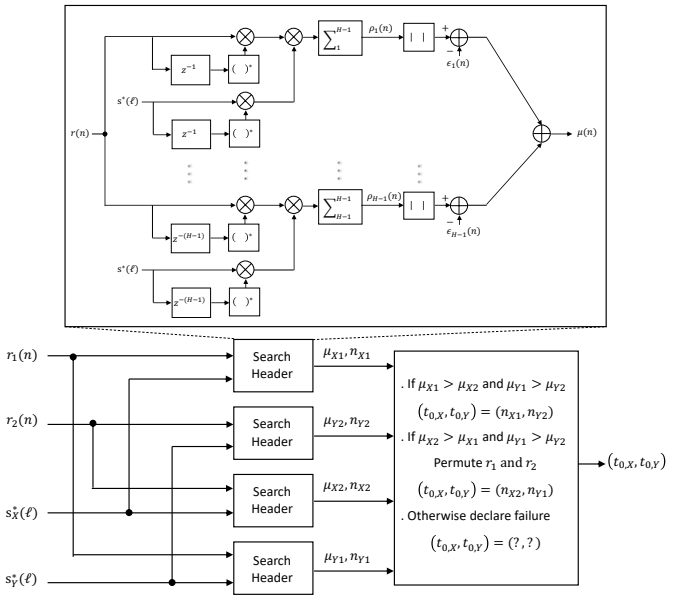

Fig. 8. Block diagram of the frame synchronizer

the same input on both outputs, entailing the loss of one polarization. Our equalizer reached steady-state convergence with proper polarization demultiplexing in less than $30\mu s$ in most simulations, even at negative SNRs. This came as a surprise for the authors which did not expect a blind algorithm to be so robust at these noise levels.

E. Frame synchronization

Frame synchronization is in charge of resolving the polarization ambiguity at the blind adaptive equalizer output, and locating the frame header on each of the two polarizations. At this stage the FSE should have taken care of any fractional delay (with respect to symbol rate) on each polarization through the two filters $(\mathbf{g_X}, \mathbf{g_Y})$. However, due to X-Y skew, there may still be a relative integer delay, multiple of the symbol rate, between the two polarizations. It follows that the search for frame headers has to be performed independently on each, to compensate and correct for this integer delay.

Frame header search uses the robust differential correlation metric proposed in [16]. In addition to being virtually immune to CFO and highly robust to laser phase noise, one can easily trade synchronization performance for hardware complexity by increasing or decreasing the maximum correlation order. Note that the correlation calculations at different orders can be carried out in parallel, and that higher-order correlations need less hardware resources than lower-orders.

The whole frame synchronization and polarisation ambiguity resolution proceeds as illustrated in Fig. 8. We search in parallel for the X and Y frame headers, on each of the X and Y signals delivered by the blind equalizer. Once a header has been detected on both polarizations, we verify that the solution is consistent, *i.e.* that we have either received X on X and Y on Y, or X on Y and Y on X. Any other situation is

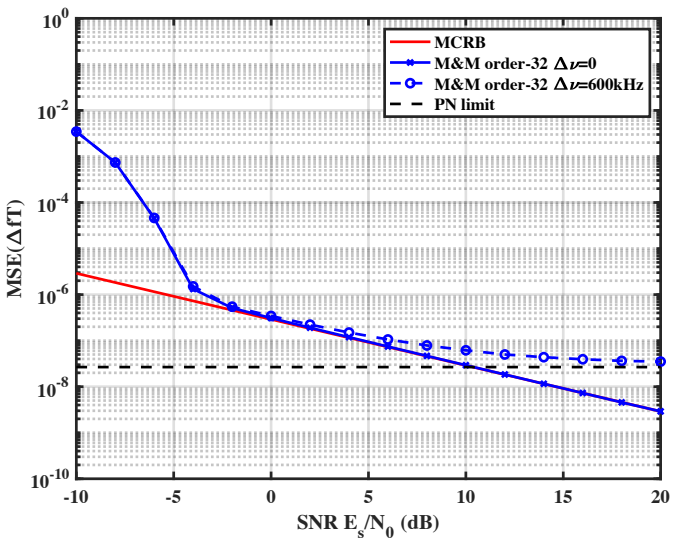

Fig. 9. Mean-square error performance of Mengali and Morelli CFO estimator with a block size of 64 symbols, a maximum correlation order of 32, with and without laser phase noise; Comparison with the theoretical limits (MCRB for AWGN only, and high-SNR MCRB limit for AWGN + PN)

regarded as a synchronization failure for the current position. A header size $H = 64$ symbols with a maximum correlation order of 32 for the synchronization metric, supplemented by a simple synchronization protocol that checks and confirms the header location within two consecutive frames, was found to be sufficient for reliable frame acquisition down to -6 dB, in less than $50\mu s$, even with 5 dB of PDL.

F. Fine carrier-frequency recovery

Fine carrier-frequency recovery uses the Mengali and Morelli data-aided frequency estimator [17]. The reason is twofold. First it has an estimation range and threshold very close to those of the maximum-likelihood data-aided estimator of Rife and Boorstyn. Second, it makes direct re-use of the correlations calculated at the frame synchronization stage, which greatly simplifies receiver design. From the simulation results in Fig. 9, which assume a block size $H = 64$ symbols with maximum correlation order $H/2 = 32$, one observes that this estimator has optimal performance at SNR > -4 dB, and acceptable performance below, with and without phase noise.

CFO estimation is performed once per frame, using the frame header. Estimation is carried out jointly on the two polarizations, for maximum accuracy (better noise averaging). The calculated frequency correction is then applied to the whole frame, and the process repeated frame after frame. Simple first-order exponential smoothing is applied to the CFO estimates from one frame to the other, in order to further improve accuracy over time.

G. Fine carrier-phase recovery

Two feed-forward carrier-phase recovery schemes very popular in the fiber-optics community are the Viterbi and Viterbi (V&V) estimator [18], and the blind phase search (BPS)

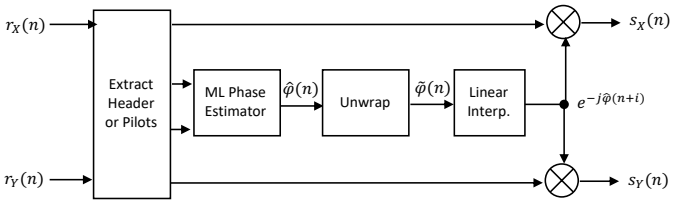

Fig. 10. Carrier-phase recovery scheme

algorithm [19]. Both allow fast tracking of phase noise in a hardware-friendly, non-data-aided manner. Our studies have shown that the performance of both approaches collapse at low SNR ($E_s/N_0 < 5$ dB). Specifically, the V&V is hindered by excessive noise amplification caused by 4-th power elevation. BPS does not have this problem, but its use of tentative decisions gives rise to catastrophic error propagation. We have chosen to work instead with pilot-based ML estimation, which is a much more robust solution, particularly at negative SNR. Simple linear interpolation between unwrapped phase estimates is used to coarsely track the phase noise variations in-between consecutive pilot blocks [20], as well as any non-negligible residual CFO that might have survived thus far. The overall carrier-phase recovery scheme is depicted in Fig. 10.

Carrier-phase estimation can be performed either independently on each polarization, or jointly. Joint estimation improves estimation accuracy by averaging over the two polarization. Equivalently, it can reduce by half the number of pilot symbols required to reach a given MSE performance, as compared to separate estimation. However joint estimation requires that both polarizations share the exact same phase offset. One can show that this assumption does not hold in the present case, due in part to X-Y skew, but also to a $\pi/2$ phase ambiguity at the output of the adaptive CMA equalizer. Fortunately it turns out that both issues can be taken care of easily, by simple prior estimation and correction of the relative phase shift between polarizations (not shown in Fig. 10), making joint phase estimation possible after all and with little additional calculation.

H. Symbol detection

Symbol detection consists in computing a soft-decision (log-likelihood ratio) on each modulated bit, for subsequent soft-decision FEC decoding.

V. Receiver Performance

The performance of the proposed receiver has been assessed under several transmission scenarios. Several performance metrics have been considered, including the uncoded bit-error rate (BER), and also the generalized mutual information (GMI), for FEC performance prediction [21]. As an illustration, Fig. 11 and 12 shows the GMI and BER measured at the DSP receiver output in the presence of various transmission impairments, and with different receiver configurations, some stages being enabled or disabled depending on the impairments. The frame size was $64 + 16 \times 256 = 4160$ symbols

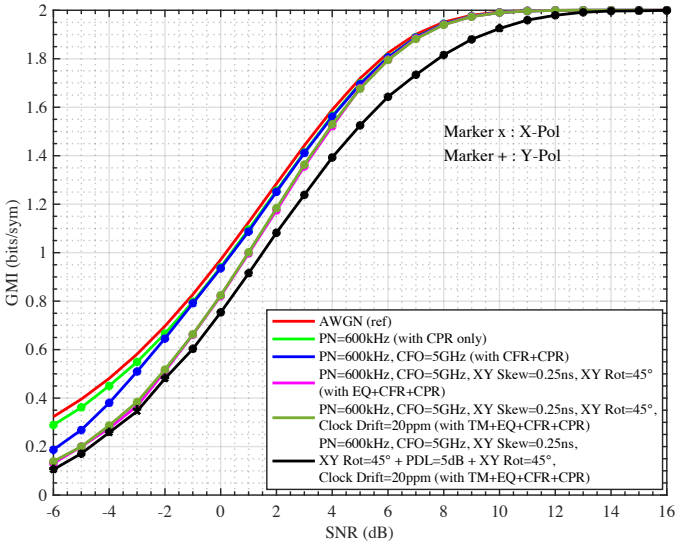

Fig. 11. Mutual information at the DSP receiver output, with different impairments and receiver configurations (PN = phase noise, CFO = carrier frequency offset, CPR = carrier-phase recovery, CFR = carrier-frequency recovery, EQ = adaptive equalizer, TM = timing recovery)

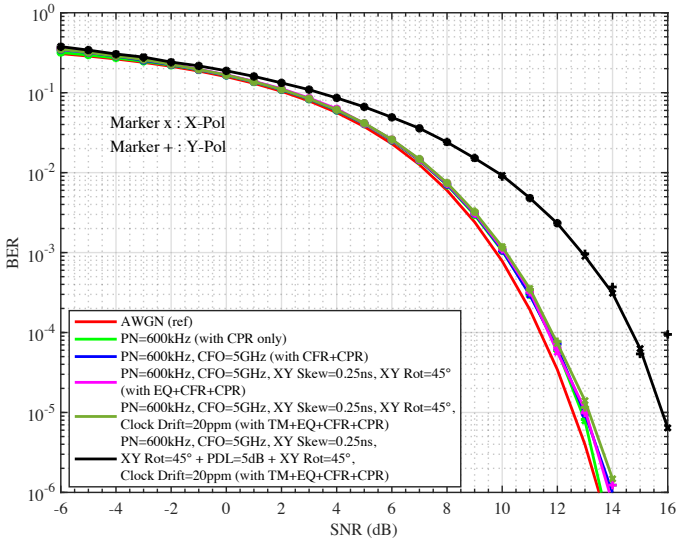

Fig. 12. Uncoded BER at the DSP receiver output, with different impairments and receiver configurations (same settings and legend than in Fig. 11)

(4.8% overhead). At every SNR, 400 frames were used for training, followed by a maximum of 300 frames for frame acquisition. BER and GMI were then evaluated over the next 512 frames.

We first verify here that blocks of 8 pilots about 256 symbols apart enable fine estimation and tracking of phase noise over the all SNR range. Switching on carrier-frequency recovery worsens the performance at negative SNR, due to the residual frequency error. The pilot symbols could be used to improve estimation accuracy and reduce this error. It is noteworthy that, in the absence of turbulence and PDL, the two main sources of degradation in communication performance are equalization noise at low-to-medium SNR, and laser phase noise at high SNR, respectively. The later was expected. The former is more surprising, and arises independently of X-Y skew or SOP rotation. It could be due to noise intrinsic to the adaptive tap coefficient update (stochastic gradient descent). One can note also that clock drifts do not hinder performance.

In the absence of PDL, we simulate a single rotation between the transmit and receive lasers SOPs. PDL simulation uses a lumped PDL model with a Jones matrix of the form $\mathbf{R}_{\theta_2}\begin{pmatrix}\sqrt{1+\gamma} & 0\\ 0 & \sqrt{1-\gamma}\end{pmatrix}\mathbf{R}_{\theta_1}$, with $\Gamma = 10\log_{10}\frac{1+\gamma}{1-\gamma}$ the PDL factor, in dB. In that case two SOP rotations occur, one before the introduction of PDL, to align with the most- and least-lossy PDL axis, and another one after, to align with the LO polarization axis. DSP alone cannot compensate for the PDL power loss, which impacts performance at all SNRs and to varying degree, depending on the first SOP rotation θ_1. In the setting in Fig. 11, the power loss distributes evenly on X and Y due to the $\theta_1 = 45°$ rotation prior to PDL introduction. This explains that the two polarization show similar BER and GMI performance in that particular case.

VI. Summary

We have demonstrated the possibility to establish reliable GEO links at an electrical SNR as low as -6 dB, in the presence of realistic system impairments, using less than 5% signaling overhead for the header and pilots. This was made possible by the design of a custom DSP receiver based on simple, proven feed-forward algorithms that borrow both from fiber-optic communication and from RF satellite communications. The proposed DSP receiver is just a proof-of-concept whose performance can be improved in many ways, *e.g.* by using the pilots to refine CFO estimation, supplementing feed-forward clock recovery by a lower-frequency feedback loop driving the ADC frequency, or by more accurate tracking of phase noise in-between pilots blocks.

These results underscore the value of a dedicated receiver architecture, both from the point of view of performance and hardware complexity (see *e.g.* equalizer simplification). However it is also worth recognizing that coherent fiber-optic DSP receivers would need little modification to reach full operational capability on GEO feeder links.

Atmospheric turbulence was not simulated, yet accounted for in the minimum operating SNR. In practice, however, deep fades will ineluctably appear and possibly span many frames. How to modify the proposed receiver so as to stay locked as long as possible in such a situation, and to recover quickly from hang-up, requires further work. Finally, albeit designed for a GEO link, the proposed frame format and DSP receiver should apply to LEO links as well with few changes.

Acknowledgment

This research was carried out under contract with the Centre National d'Etudes Spatiales (CNES). The authors would like to thank Yves Jaouen from Telecom Paris and Géraldine Artaud from CNES for many fruitful discussions.

REFERENCES

[1] B. Roy *et al.*,"Optical feeder links for high throughput satellites," in *Proc. 2015 IEEE Int. Conf. on Space Optical Systems and Applications (ICSOS)*, New Orleans, LA, USA, 26–28 Oct., 2015, pp. 1-6.

[2] R. Mata Calvo, D. Giggenbach, A. Le Pera, J. Poliak, R. Barrios, and S. Dimitrov, "Optical feeder links for very high throughput satellites – System perspectives," in *Proc. 2015 Ka and Broadband Commun., Navigation and Earth Obs. Conf.*, Bologna, Italy, 12–14 Oct., 2015.

[3] Curt M. Schieler *et al.*, "On-orbit demonstration of 200-Gbps laser communication downlink from the TBIRD CubeSat," *SPIE Proc. Vol. 12413, Free-Space Laser Free-Space Laser Commun. XXXV*, Mar. 2023.

[4] P. Conroy, J. Surof, J. Poliak, and R. M. Calvo, "Demonstration of 40 Gbaud intradyne transmission through worst-case atmospheric turbulence conditions for geostationary satellite uplink," *Applied Opt.*, vol. 57, no. 18, pp. 5095–5101, June 2018.

[5] D. J. Geisler, "Coherent architectures for free-space optical communications," in *Proc 2020 Conf. on Lasers and Electro-Optics (CLEO)*, San Jose, CA, USA, 10–15 May 2020.

[6] M. Torbatian *et al*., "Performance oriented DSP for flexible long haul coherent transmission," *J. Lightw. Technol.*, vol. 40, no. 5, pp. 1256–1272, 1 Mar. 2022.

[7] R. Nagarajan, I. Lyubomirsky and O. Agazzi, "Low power DSP-based transceivers for data center Ootical fiber communications," *J. Lightw. Technol.*, vol. 39, no. 16, pp. 5221–5231, Aug. 2021.

[8] *Digital Video Broadcasting (DVB); Second Generation Framing Structure, Channel Coding and Modulation Systems for Broadcasting, Interactive Services, News Gathering and other Broadband Satellite Applications*, ETSI Std., Rev. ETSI EN 302 307 V1.3.1, Mar. 2013.

[9] *Implementation Agreement 400ZR*, Optical Internetworking Forum (OIF) Std., Rev. IA OIF-400ZR-01.0, Mar. 2020.

[10] U. Mengali and A. N. D'Andrea, *Synchronization techniques for digital receivers*. Kluwer Academic Publishers, 1997.

[11] S. J. Lee, "A new non-data-aided feedforward symbol timing estimator using two samples per symbol," *IEEE Commun. Lett.*, vol. 6, no. 5, pp. 205–207, May 2002.

[12] Y. Wang, E. Serpedin, and P. Ciblat, "An alternative blind feedforward symbol timing estimator using two samples per symbol," *IEEE Trans. Commun.*, vol. 51, no. 9, pp. 1451–1455, Sep. 2003.

[13] M. S. Faruk and S. J. Savory, "Digital signal processing for coherent transceivers employing multilevel formats," *IEEE Trans. Learn. Technol.*, vol. 35, no. 5, pp. 1125–1141, Mar. 2017.

[14] K. Kikuchi, "Polarization-demultiplexing algorithm in the digital coherent receiver," in *Proc 2008 Digest of the IEEE/LEOS Summer Topical Meetings*, Acapulco, Mexico, 2008, pp. 101-102.

[15] O. Zia-Chahabi, R. L. Bidan, M. Morvan, and C. Laot, "Efficient frequency-domain implementation of block-LMS/CMA fractionally spaced equalization for coherent optical communications," *IEEE Photon. Technol. Lett.*, vol. 23, no. 22, pp. 1697–1699, Nov. 2011.

[16] D.-U. Lee, P. Kim, and W. Sung, "Robust frame synchronization for low signal-to-noise ratio channels using energy-corrected differential correlation," *EURASIP J. Wireless Com. Network.*, 2009.

[17] U. Mengali and M. Morelli, "Data-aided frequency estimation for burst digital transmission," *IEEE Trans. Commun.*, vol. 45, no. 1, pp. 23–25, Jan. 1997.

[18] A. J. Viterbi and A. M. Viterbi, "Nonlinear estimation of PSK-modulated carrier phase with application to burst digital transmission, " *IEEE Trans. Inform. Theory*, vol. 29, no. 4, pp. 549–551, July 1983.

[19] X. Zhou, "Efficient clock and carrier recovery algorithms for single-carrier coherent optical systems: A systematic review on challenges and recent progress," in *IEEE Signal Process. Mag.*, vol. 31, no. 2, pp. 35–45, March 2014.

[20] E. Casini, R. De Gaudenzi, and A. Ginesi, "DVB-S2 modem algorithms design and performance over typical satellite channels", *Int. J. Sat. Commun. and Netw.*, vol. 22, pp. 281—318, 2004.

[21] A. Alvarado, E. Agrell, D. Lavery, R. Maher and P. Bayvel, "Replacing the soft-decision FEC limit paradigm in the design of optical communication systems," *J. Lightw. Technol.*, vol. 34, no. 2, pp. 707–721, Jan. 2016.